Planar Magnetometers

Asif I. Zia and Subhas C. Mukhopadhyay

Abstract The increasing demand of miniaturization, low power consumption, compactness and portability of the equipment has urged the sensors' size to be the only selection criterion for a magnetometer. Applications, such as magnetic micro-beads, micromagnetic scanning, non-destructive testing and medical applications like magnetic drug delivery dictate the requirement of magnetic sensors that are smaller in size and own single side measurement capability. To cater those needs, it is utmost important to explore and apply new principles governing nano-scale science and state-of-the-art fabrication technology. This chapter showcases the recent advances in magnetic field planar sensors that could be used to measure magnetic field with the privilege of non-destructive measurements and single side access to the sample.

1 Introduction

Magnetometers are defined as sensitive electronic readout instruments, equipped with specialized sensors that are used either to measure the magnetization of magnetic materials or measure the strength and direction of magnetic fields at a given point in space. The magnetic-field sensors are the core devices that operate on many physical, electronic, electrical and optical principles including magnetic induction, Lorentz force, Faraday rotation, Hall Effect, and magneto-optical effects. Contemporary techniques applied for magnetic sensing exploit wider areas in the fields of physics and material science. Recent progress in precise control of feature

A.I. Zia (✉) · S.C. Mukhopadhyay
School of Engineering and Advanced Technology, Massey University,
Palmerston North 4442, New Zealand
e-mail: a.i.zia@me.com

S.C. Mukhopadhyay
e-mail: s.c.mukhopadhyay@massey.ac.nz

A.I. Zia
Department of Physics, COMSATS University, Park Road, Islamabad, Pakistan

A. Grosz et al. (eds.), *High Sensitivity Magnetometers*, Smart Sensors,
Measurement and Instrumentation 19, DOI 10.1007/978-3-319-34070-8_12

size using hi-tech lithography techniques in semiconductor industry has paved the way to the successful fabrication of thick and thin film magnetic sensors and related transducers. State-of-the-art modern micromachining techniques have facilitated new types of solid-state microelectromechanical systems (MEMS) that provide versatile solutions to many problems normally associated with similar structures at larger scales. These systems are capable enough to replace bulky three dimensional systems with planar miniature systems. The reduction in fabrication cost in turn leads to a wide range of high precision magnetic sensor types. These include planar induction coil, fluxgate, SQUID, Hall-effect, anisotropic magneto-resistance (AMR), giant magneto-resistance (GMR), magnetic tunnel junctions, giant magneto-impedance, magnetostrictive composites, magnetodiode, magnetotransistor, fiber optic, magneto-optic, optically pumped, nuclear precession, and MEMS based magnetic sensors. This chapter reviews and discusses the advancements in miniaturization and transformation of bulky magnetic sensors into smart sensing devices. Applications of planar meander and mesh coils based magnetic sensors would also be discussed in due course.

2 Background

A magnetic sensor interprets magnetic field into electrical signals; therefore the general principle of operation of a magnetic transducer is either based on alternating current or direct current applications. Figure 1 shows a family tree of magnetic

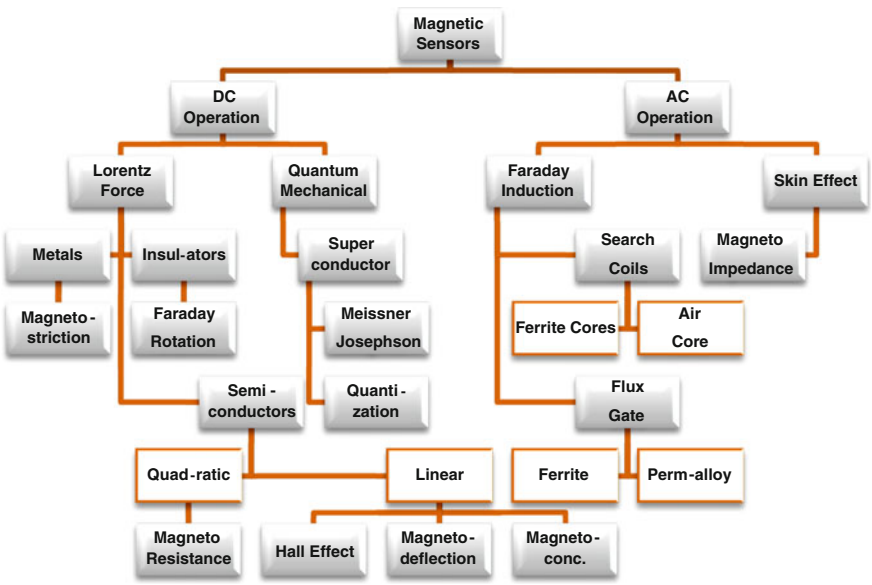

Fig. 1 Family tree of magnetic sensor materials and effects

sensors and materials segregated on the basis of type of exposed excitation and the consequent galvanomagnetic effects produced. The most fundamental of all galvanomagnetic effects is the Hall Effect that is responsible for the generation of an electric field orthogonal to the magnetic induction vector when a direct current flows through a conductor in the direction perpendicular to both. In case of current flowing through a superconducting material the galvanomagnetic effect observed at the Josephson junctions is termed as quantum mechanical galvanomagnetic effect that has become the foundation for realization of highly sensitive SQUID (superconducting quantum interference device) sensors and magnetometers [1].

3 Mathematical Model Based Physical Principles of Operation

Following discussion gives a brief account of some physical principles used to develop planar magnetic sensors and magnetometers operating on direct current technology.

Under the action of Lorentz force and Coulomb force, the phenomena of charge-carrier transport in conducting or superconducting material gives rise to the galvano-magnetic effects governed by the following relation.

$$F = eE + e[v \times B] \tag{1}$$

where 'e' denotes the carrier charge (for electrons $e = -q$, and for holes $e = +q$ and $q = 1.6 \times 10^{-19}$ °C), E denotes the electric field, $\boldsymbol{v}$ the carrier velocity and B the magnetic induction. For non-degenerate semiconducting materials exposed to the transverse electrical and magnetic fields (i.e. $E \cdot B = 0$), the current transport equation in terms of total current density 'J' is given by [2]:

$$J = J_0 + \mu_H[J_0 \times B] \tag{2}$$

where J_o is the carrier charge density due to electric field with a carrier concentration gradient ∇n given in (3). The transport coefficients μH (the Hall mobility which has the sign of the corresponding charge-carrier), σ (the conductivity), and D (the diffusion coefficient) are determined by the carrier scattering processes and generally depend on electric and magnetic fields.

$$J_0 = \sigma E - eD\nabla \mathrm{n} \tag{3}$$

Both the Hall and the magneto-resistive effects can be derived from the solutions of Eq. (2) subject to the application of appropriate boundary conditions [3].

3.1 Hall Effect and Magneto Resistivity in Semiconductors

Consider a special case of carrier transport in a very long narrow strip of an extrinsic and homogeneous ($\nabla n = 0$) semiconductor material along x-axis that is exposed to a magnetic field of known magnetic flux density along y-axis $B = (0, B_y, 0)$. If the strip is exposed to an external electric field $E_x = (E_x, 0, 0)$, a current I will flow through it with current density $J = (J_x, 0, 0)$. Since $J_z = 0$, an internal transverse electric field $\boldsymbol{E}_H$ known as the Hall field must build up in order to counteract the Lorentz force, that can be determined from Eq. (2) by substituting $E = E_x + E_H$, under the condition that the transverse current density vanishes, i.e. $E_H = (0, 0, E_z)$ and $E_z = -\mu_H B E_x$. The appearance of Hall field gives rise to a measurable transverse voltage called Hall voltage V_H that can be calculated as (ignore–sign):

$$V_H = \mu_H E_x B w = R_H J_x B w \tag{4}$$

where w is the strip width. $R_H = \mu_H/\sigma = r/en$ is called the Hall coefficient and r *is* the Hall scattering factor of carriers with n carrier density. In semiconducting materials low carrier density results into a large Hall coefficient; therefore, Eq. (4) explains the superiority of semiconductors over conductors. The deflection of the resultant electric field occurs due to the generation of the Hall Field, that is evaluated in terms of Hall angle measured with respect to the applied external field. Where $\tan \theta_H = E_z/E_x = -\mu_H B$.

A rotation in the electric field lines by θ_L called Lorentz deflection angle is described by a ratio in Eq. (5). It is observed when a short strip of wide cross-sectional area is exposed to the external electric field $E_x = (E_x, 0, 0)$.

$$\frac{J_z}{J_x} = \mu_H B = \tan \theta_L \tag{5}$$

The consequent current density leads to a lateral component J_z that is responsible for longer drift path of the carriers giving rise to geometric magneto-resistance effect mathematically expressed by Eq. (6) [2].

$$\frac{\rho_B - \rho_o}{\rho_o} = (\mu_H B)^2 \tag{6}$$

where ρ_0 represents the electrical resistivity at $B = 0$, and ρ_B the increased resistivity due to the presence of the magnetic field. Equation (6) provides the relative change in resistivity. Due to low carrier mobility, intrinsic silicon does not display considerable amount of magneto-resistivity effect. Magnetic sensors based on this effect require high-mobility narrow band-gap III–V compounds such as Indium Antimonide or Indium Arsenide semiconductors [4].

3.2 Anisotropic Magneto-Resistance

Anisotropic magneto-resistance is an intrinsic property observed in ferromagnetic transition metals and alloys. Permalloy is an alloy containing about 80 % nickel and 20 % iron, exhibit anisotropic magneto-resistance. The magnetization vector determines the direction of current flow in these materials; therefore, when exposed to an external magnetic field the resultant magnetization vector rotates the current path, by an angle θ [5]. The specific resistivity of the sample as a function of θ, $\rho(\theta)$, is given by Eq. (7):

$$\rho(\theta) = \rho_{\perp} + \left(\rho_{||} - \rho_{\perp}\right) \cos^2 \theta = \rho_{\perp} + \Delta\rho \cos^2 \theta \tag{7}$$

where $\rho\|$ is the resistivity of the sample when current flow is parallel to magnetization vector i.e. $\theta = 0$, $\rho\perp$ the resistivity of the sample when current flow is perpendicular to magnetization vector $\theta = 90°$. The magneto-resistive effect $(\Delta\rho/\rho_o)$ is the ratio of change in resistivity to the resistivity at $\theta = 0$. The advances in thin-film deposition technology have paved the way to use anisotropic magneto-resistance effect in magnetic sensor applications [6].

3.3 Flux Quantization-Meissner Effect

The constancy of magnetic flux consequent to flux quantization inside a superconducting closed loop is known as Meissner effect. The magnetic sensors using superconducting materials and applying Meissner effect to measure magnetic field are commonly known as SQUID magnetometers. A closed superconducting loop when placed in an external magnetic field induces a shielding current, known as the super-current I_s, that circulates around the inner surface of the ring such that the total magnetic flux, Φ_i, inside the ring is quantised. Equation (8) provides the magnitude of the quantized flux in terms of self-inductance L of the superconducting closed loop, induced current I_s and external field flux Φ_e.

$$\phi_i = m\phi_o = LI_s + \phi_e \tag{8}$$

where $\Phi_0 = 2.07 \times 10^{-15}$ Wb is the flux quantum and m a multiple integer. Any variation in the external flux is responded by the superconducting loop by an equal but opposite flux as long as the super-current I_s stays within a critical limit of the current value termed as I_c. The current I_s through the superconducting loop is measured using Josephson junctions that provided means to development of highly sensitive SQUID magnetometer.

Alternating current based magnetic sensing uses the physical principles of classical electrodynamics. Planar magnetic sensors like search-coil sensors, fluxgate

sensors and magneto impedance and giant magneto-impedance sensors have been developed using Faraday's law of induction and electromagnetic theories. For ac excitation the voltage V is related to the resulting current I via complex impedance Z which is a function of skin-depth δ that depends on the angular frequency ω and magnetic permeability of the material. Equation (9) and (10) describe the mathematical interpretation of V and I.

$$V = Z(\delta)I \tag{9}$$

$$I = I_o \exp(i\omega t) \tag{10}$$

where I_o is the amplitude

4 Planar Integrated Micro Hall Sensor

Hall Effect is the most applied physical phenomenon for the magnetic sensors [7]. The Hall sensitivity of silicon ranges from 10 to 1000 G or 10^6–10^8 nT and the sensitivity of Hall sensors is typically 1 mV/mT for a 1 mA current. Hall Effect devices have achieved a high number of low cost position sensing applications. They are lightweight planar devices and consume power between 0.1 and 0.2 W and can operate safely over a wide temperature range. Hall Effect sensors can measure either a constant or a varying field with an upper frequency limit at about 1 MHz. For higher sensitivity applications thin-film of Indium Antimonide (InSb) with a typical sensitivity 5 mV/mT and Indium Arsenide (InAs) with a typical sensitivity of 2 mV/mT are used [8]. InAs exhibits better temperature stability of the Hall voltage in comparison to Silicon and InSb. InAs Hall effect sensors can operate in a range of −40 to +150 °C which declares them the best candidates for automotive applications [9]. A promising Hall sensor was made using silicon-on-insulator (SOI) technology: 1μT/$\sqrt{\text{Hz}}$@1 Hz noise was achieved for an 80-μm wide, 50-nm thick sensor [10]. Two-dimensional quantum-well multilayer heterostructures based on GaAs are promising for low-noise Hall sensors: 100nT/$\sqrt{\text{Hz}}$@1 Hz noise was achieved with external spinning-current electronics, which was further improved threefold by using leakage-free switches [11].

Figure 2 shows an off-the-shelf planar InSb Hall sensor. The InSb thin-film Hall sensor is sandwiched between two ferrite pieces with an integrated ferrite concentrator (Asahi Kasei, BW series). The figure shows the FEM simulated flux lines and a micro-photograph of the device [8].

A new microsystem based on the non-invasive Hall principle was published recently. The system owned the ability to detect magnetic microstructures [12]. The micro-Hall plate had an active area of only 2.4 μm × 2.4 μm that is embedded in the microsystem fabricated by applying CMOS technology. The microsystem exhibited a magnetic field resolution of 300 nT/$\sqrt{\text{Hz}}$ at 1 Hz. A two-dimensional

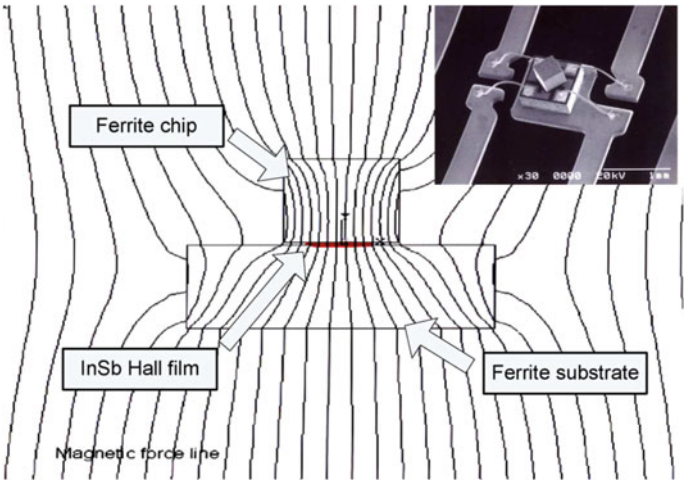

Fig. 2 Magnetic force lines of field concentrators for a thin-film Hall sensor (FEM simulation [8])

magnetic scanner was developed to demonstrate the performances of the developed microsystem [12]. The microsystem displayed its ability to compensate the temperature dependence of the sensor and the magnetic circuit enclosing the sensor by embedding the sensor on a planar CMOS chip with dimensions 2600 µm by 900 µm.

The micro-Hall plate sensor is placed in the peripheral corner of the silicon chip as depicted in Fig. 3. The bonding connections are placed on the opposite side of the chip far away from the Hall sensor to minimize the noise. Such planar design allows non-invasive single side access of the Hall sensitive area to the surface required to be magnetically characterized.

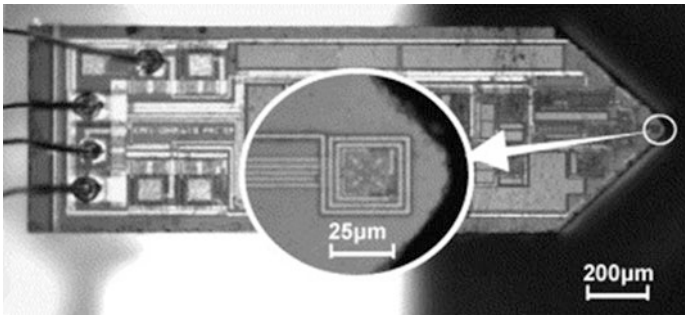

Fig. 3 Photograph of the integrated micro-Hall probe. The micro-Hall plate sensor is placed in the peripheral corner of the silicon chip. Chip dimensions are 2600 µm × 900 µm [12]

5 Planar Anisotropic Magneto-Resistance (AMR) Sensors

Permalloy is probably the most common material for AMR sensors due to its relatively larger magneto-resistance. The other merit points of using Permalloy as AMR sensor are its characteristics compatibility with the applied fabrication techniques employed to make silicon integrated circuits such as a zero coefficient of magnetostriction and ease of thin film deposition [5]. A planar AMR integrated sensor comprises of a bridge configuration of four Permalloy resistors. The fabrication is normally achieved by sputtering process that deposits the bridge in form of thin film on a silicon substrate. A potential difference develops between the two paths of current if there is a mismatch of resistance between the two paths. Longer current path designs ensure high bridge resistance consequently reducing the power requirement of the AMR sensor [8]. A precise resistance match is required for all four bridge resistors in order to avoid any offset potential difference to appear across the two paths of current flow in the absence of test magnetic field. Special design and fabrication methodologies are adopted to reduce the offset potential difference appearing from mismatches in the four resistors.

Figure 4 [13] shows an image of planar design for AMR chip sensor with four Resistor Bridge. Two meander coils are fabricated in order to provide feedback field and a set/reset field.

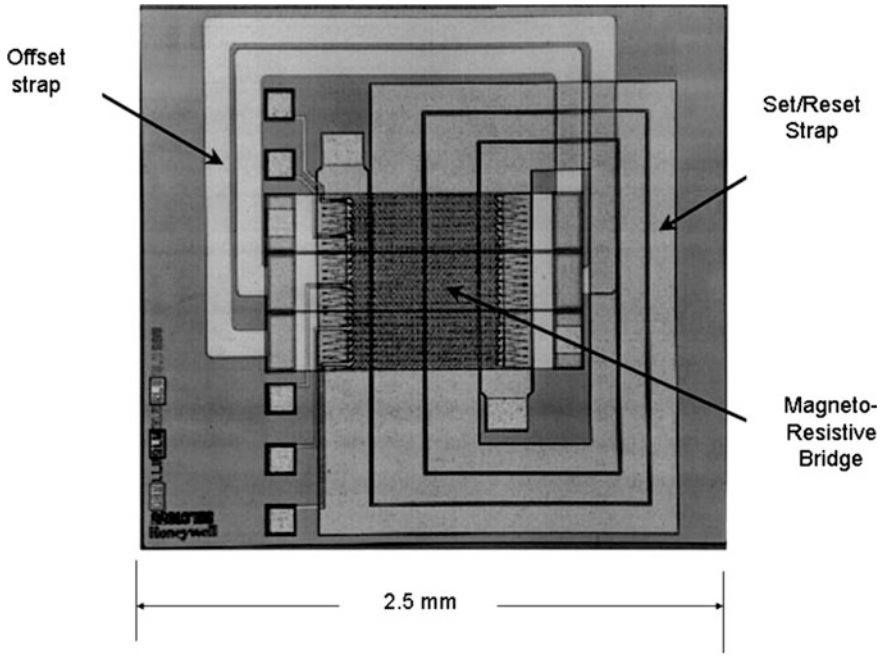

Fig. 4 Planar design configuration of an AMR sensor displaying four resistors bridge, and two coils, (i) for set/reset field pulses and, (ii) for feedback field [13]

The recent fabrication advancement in semiconductor fabrication industry has made it viable to fabricate the magnetometer readout electronics and additional temperature-compensating circuitry on the same chip. To achieve linearity between changes in resistance corresponding to change in the magnetic field, the biasing of the bridge is applied to rotate the direction of magnetization. A thin film of cobalt is sputter-coated over the resistors to provide shorting paths on the Permalloy strip. On magnetizing cobalt, magnetic field causes the current to direct at an angle of 45 relative to the direction of magnetization that appears as a barber pole [4].

The AMR planar sensors have a sensitivity range of 10^{-2} to 50 G or 10^{3} to 5×10^{6} nT with open-loop readout electronics [13]. For limited bandwidths and applying closed-loop feedback readout electronic methods, a minimum detectable field of 0.1 nT can be achieved.

AMR sensors based magnetometers own an outstanding capability to measure magnetic field strength over an extremely wide dynamic range from 0 Hz to nearly 1 GHz. These sensors are lightweight, miniaturized in size and require merely up to 0.5 mW of power. The operating temperatures normally are between 55 and 200 °C [14].

6 Planar Fluxgate Magnetic Sensors

A recent publication presented a novel class of miniature fluxgate magnetometers fabricated on a printed circuit board (PCB) substrate and electrically connected to each other similar to the current "flip chip" concept in semiconductor package. The proposed sensor was soldered together by reversely flipping a 5 cm × 3 cm PCB substrate to the other identical one which included dual magnetic cores, planar pick-up coils, and 3-D excitation coils constructed by planar Cu interconnections patterned on PCB substrates [15]. Schematic of the proposed flip-chip micro-fluxgate sensor is shown in Fig. 5.

The main components and the final assembly of the "flip chip" fluxgate sensor are shown schematically in Fig. 6.

The sensor's operation has been characterized by employing the improved second-harmonic detection technique that enabled linear *V-B* correlation and responsivity verification. Additionally, the double magnitude of responsivity measured at very low frequency (1 Hz) magnetic fields had been experimentally demonstrated. The maximum responsivity of 593 V/T at 50 kHz of excitation frequency with the second harmonic wave of excitation was concluded; however, the minimum magnetic field noise was found to be 0.05nT/$\sqrt{\text{Hz}}$ @ 1 Hz for the mentioned excitation potential [15].

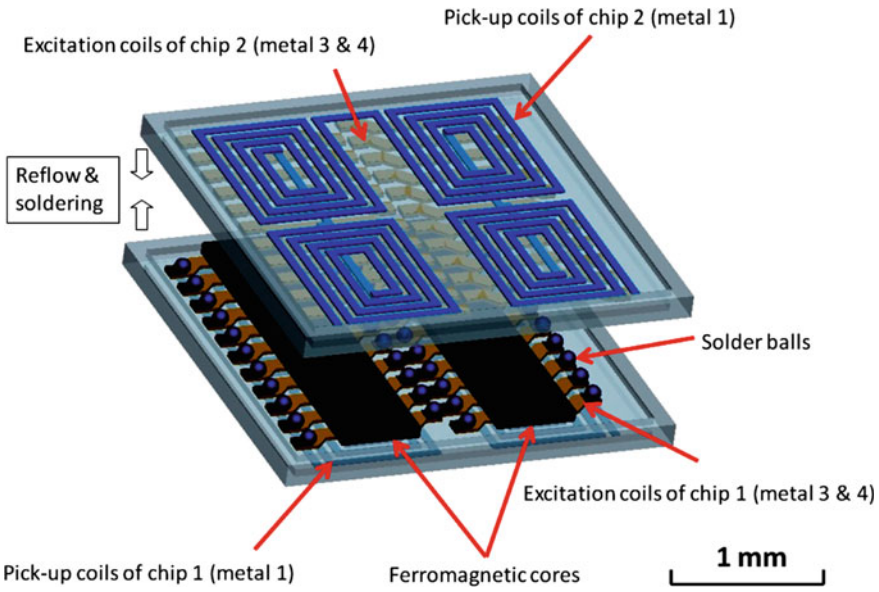

Fig. 5 Shematic of the proposed flip-chip micro-fluxgate sensor [15]

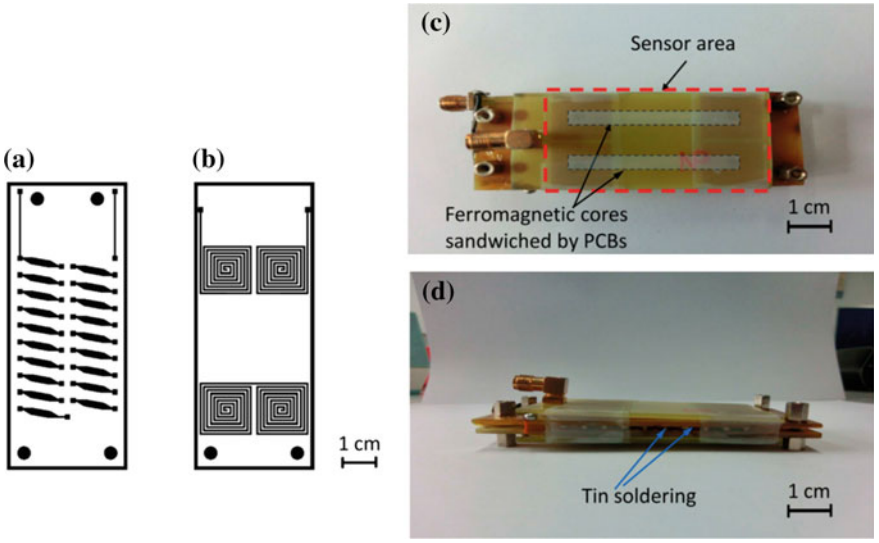

Fig. 6 **a** Cu patterns of the excitation coil on PCB substrate (*front side*); **b** Cu patterns of the pick-up coil on PCB substrate (*back side*); **c** top view and **d** side view of the completed "flip-chip" fluxgate sensor [15]

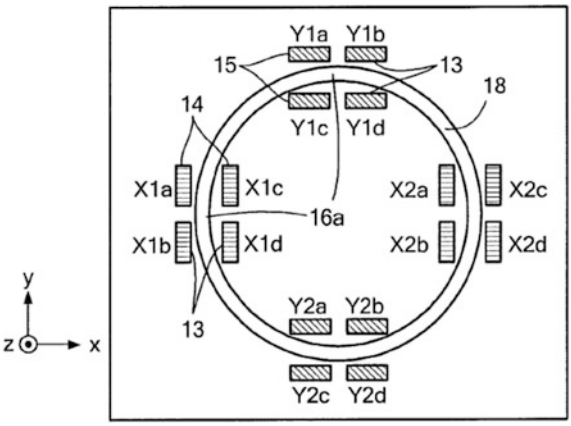

Fig. 7 View of the three axis planar magnetic field sensor with ring shaped magnetic concentrator [16]

7 Planar Three-Axes GMR Magnetometer

A planar three axis sensor has been patented in October 2013 for sensing magnetic flux along three mutually orthogonal axes. The proposed magnetometer can be used for three dimensional magnetic sensing and other magnetic field sensing applications. The sensing units operate to sense X and Y axis magnetic flux signals in the device XY-plane, While Z axis sensitivity has been achieved by use of a continuous ring shaped or octagonal magnetic concentrator that has been adapted to transform the Z axis magnetic flux signal into magnetic flux signals into the XY-plane

Referring to Fig. 7, magnetometer layout in accordance with the presented design shows a continuous, ring-shaped magnetic concentrator. The magnetic concentrator is formed of a ferromagnetic material having high permeability and low coercive force. The GMR and/or TGMR units 14 and 15 (Fig. 7) on each side of the magnetic concentrator are structurally identical. The units 14 and 15 are disposed on opposite sides of concentrator. A set/reset coil arrangement had been used for initiating, setting, and resetting the magnetization directions of the free layer and the magnetic concentrator. With multiple groups of sensing units for the XZ plane and multiple groups of sensing units for the YZ plane, it was made possible to acquire a differential signal for Z from one of the sensing units and a composite signal for X or Y from another sensing units [16].

8 Planar Induction Coil Sensors

Induction coil sensors commonly called search coil and pickup coil sensors are the oldest and well-researched types of magnetic sensors operating on alternating current technology. The transfer function governing the magnetic sensing $V = f(B)$ results from the fundamental Faraday's law of induction. The transfer impedance is defined as the ratio of the induced voltage across the sensing coil to the

current of the exciting coil. The exciting winding carries time varying (high-frequency) magnetic field to inspect non-conducting magnetic media in which no eddy-currents are induced, as well as to inspect conducting media, such as metal, in which eddy currents are induced [17]. The planar type configuration being flexible is suitable for curved surfaces and can be used for the inspection of cooling pipes used in nuclear power station and also the aircraft's surface etc.

Many research papers have been reported for the determination of near-surface material properties using the measured frequency-dependent impedance of a small right cylindrical air-core coil placed next to the metal surface and driven by an alternating current [18–22]. Usually the electromagnetic properties of the test material, including its defects, are inferred from the changes in the coil impedance caused by the presence of the test material [23, 24]. The normalized values of resistive component, R_n, and the reactive component, X_n are used and are given by,

$$R_n = \frac{R_m - R_o}{R_o} \quad and \quad X_n = \frac{X_m}{X_o} \tag{11}$$

where R_m, and X_m, are the real and imaginary components of the impedance when the sensor is coupled to the material and R_o and X_o are the corresponding air, or uncoupled values. The experimental results indicate that the shapes of the normalized impedance diagrams of ferrite pot core eddy current sensors are independent of sensors design parameters, lift-off, and material resistivity [18].

Planar type meander coils have been used for the evaluation of near-surface properties and are reported in [25, 26]. The aim is to extend the modelling technique to planar mesh type sensors and to investigate the feasibility of applying it to estimate the near-surface material properties and the quality inspection of structural health and crack determination [27], electroplated materials [17], fat contents in dairy products [28], saxophone reeds [29] and nitrate contamination in potable water [30].

8.1 Configuration of Planar Induction Coil Sensors

There are two types of planar electromagnetic sensors commonly used for performance evaluation of material properties for non-destructive evaluation and single side access of the magnetic material under test. The type of test material dictates the sensor-type chosen for the particular application. Figure 8a, b show the configuration of meander and mesh type planar induction coil sensors. The meander and mesh sensors consist of two planar coils; an excitation coil (meander type) and a sensing coil (mesh type) with mesh planar coil placed on top of meander coil with insulation sandwiched between the two planar configurations. The meander coil is energised by a high-frequency sinusoidal perturbation that induces an electromagnetic field in the test material. The material-induced field interacts with the

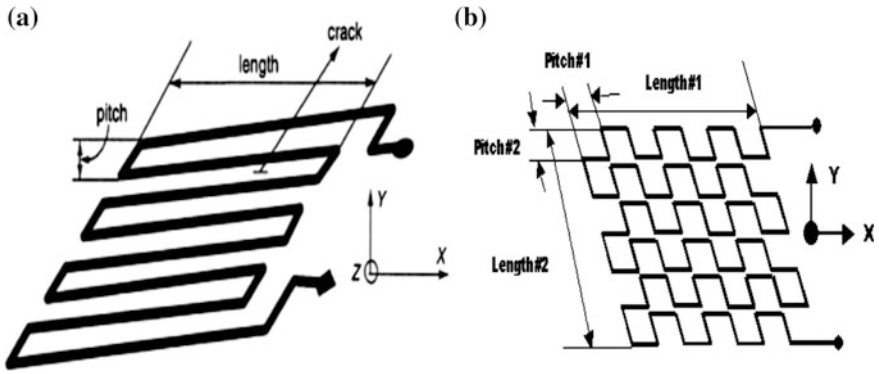

Fig. 8 Configuration of planar electromagnetic sensors. **a** Meander type. **b** Mesh type [29]

applied field and the resultant field is picked up by the planar mesh coil placed above the exciting coil.

The meander and the mesh planar configurations are separated by a polyimide film of 50 μm thickness. To improve the magnetic flux penetration in the test-material, a magnetic plate of N_iZ_n is placed on top of the sensing coil. The size of the sensor depends on the number of pitches used in it. The optimum pitch size depends on the application. The size used in this application is 27 × 27 mm, with a pitch size of 3.25 mm. The sensitivity of the meander-type sensor varies with its orientation with respect to the test-material. Hence, in some applications the mesh

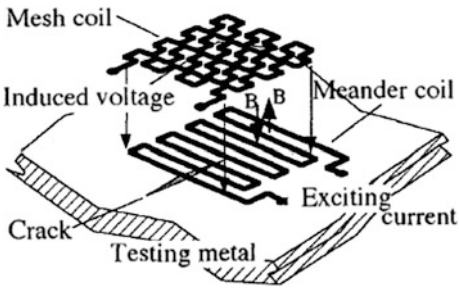

Fig. 9 Configuration of meander/mesh coupled eddy current testing probe [27]

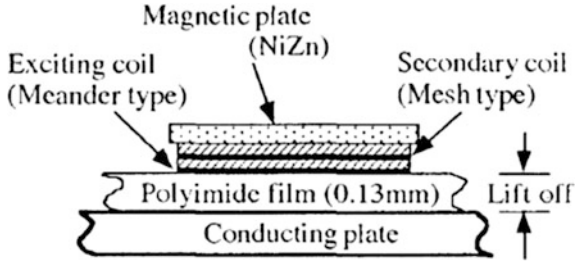

Fig. 10 Cross section of the planar eddy current test probe (ETC) [27]

type is more appropriate. The structural configuration of these sensors is shown Fig. 9. Figure 10 shows the cross-sectional view of the sensor applied for crack determination in a metallic plate.

8.2 *Finite Element Modelling of Mesh and Meander Coils*

The electromagnetic field distribution of mesh and meander configurations of planar sensors was analysed with the help of finite-element analysis tools. Comsol Multiphysics FEM software was used to deduce the critical parameters in addition to magnetic field distributions for the designed planar sensors. Figures 11 and 12 show the screen-shots of the magnetic field distribution across meander and mesh-type planar sensors, respectively.

The software uses mathematical models and Maxwell's equations to deduce important numerical parameters for the simulated design of the magnetic sensor. Based on provided boundary conditions and calculated parameters the software plots the expected magnetic field distribution around the sensors. It was observed that the magnetic flux lines enter the horizontal plane (*Z*-axis) perpendicularly and come out for both sensors. The distribution affects only one axis (parallel to horizontal plane) for the meander type, whereas for the mesh type, the distribution affects both axes of the horizontal plane.

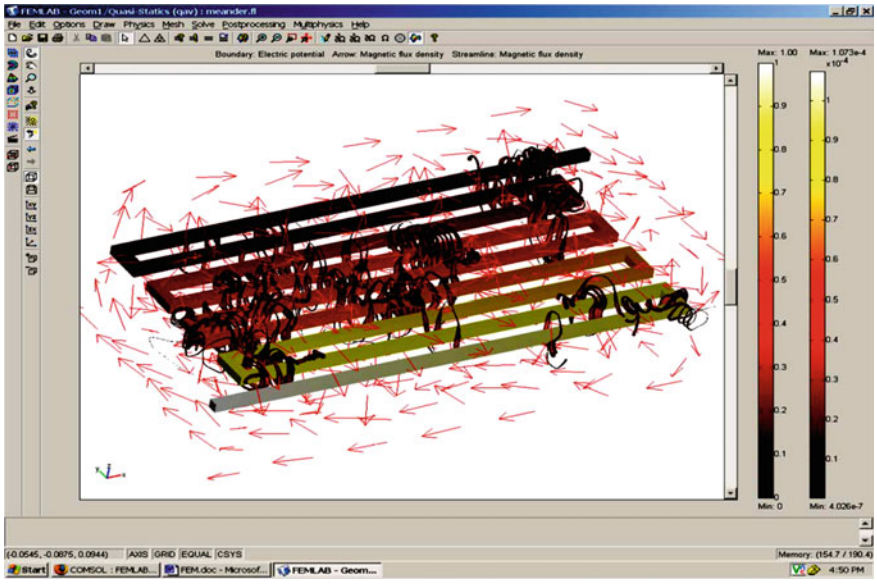

Fig. 11 Magnetic field distribution for meander planar sensor mathematically deduced by COMSOL FEM software [29]

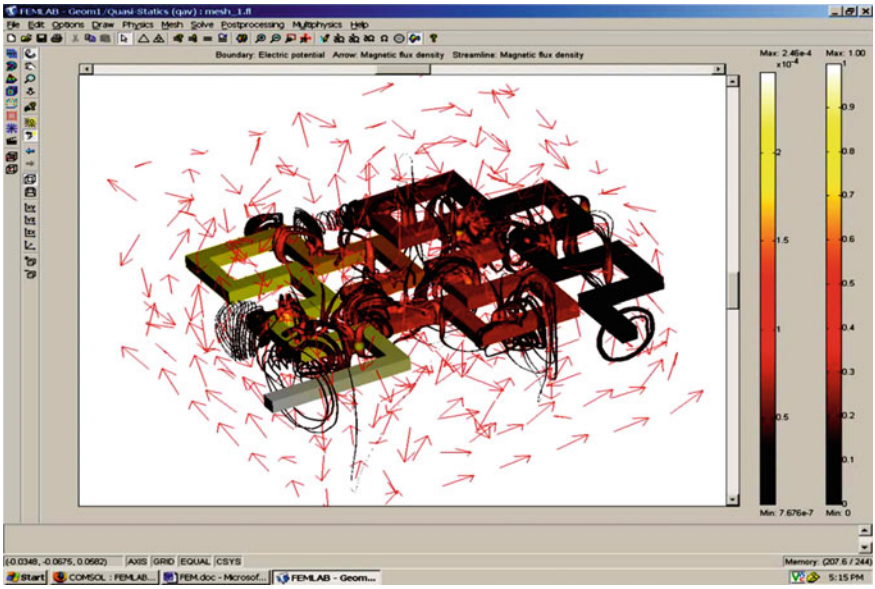

Fig. 12 Magnetic field distribution for meander planar sensor mathematically deduced by COMSOL FEM software [29]

8.3 Planar Meander and Mesh Sensors' Fabrication

All sensors were designed using the Altium Designer 6.0. The FR4 substrate sensors were fabricated at Massey University using standard PCB printing technology. The design was laser-printed on transparency film. The photo-resist board was used. The conducting layers of the board are typically made of thin copper foil. The film together with the board was exposed to the UV light. This process will impress and burn the desired sensor design onto the board. The photo-resist board was then placed in a tank filled with developer. Then, the board was immersed into a special chemical for etching process to remove the unwanted copper, leaving only the desired copper trace. The sensors were cut into a suitable design for testing [31, 32].

9 Applications of Meander-Mesh Planar Sensors

9.1 Defect Imaging by Planar ECT Probe

Advanced planar type eddy current testing probe (ETC) had been developed for detecting cracks/defects in metallic objects. The key idea for this probe is the induction of eddy currents inside a conductive plate on application of alternating

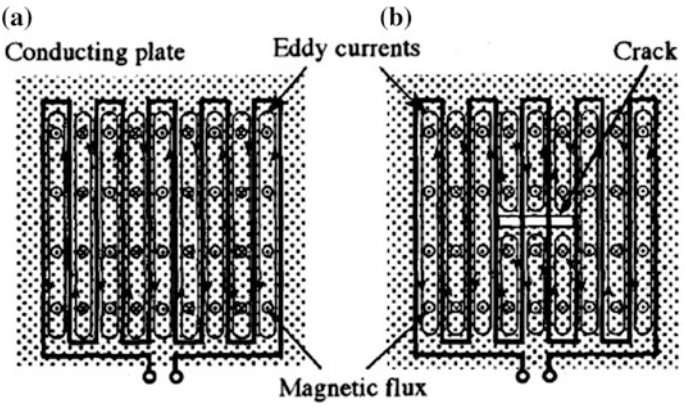

Fig. 13 Distribution of induced magnetic flux and eddy currents [27]

magnetic field produced by the meander coil. The mesh coil is a two-dimension pick up coil that senses a localized magnetic field generated by rotating currents in the conductive plate. With no defects the magnetic fields produce regular patterns and thus eddy currents have the direction at each pitch as shown in Fig. 13a. In other case, the distribution of eddy currents has localized patterns if defects exist as shown in Fig. 13b.

Imaging technology can further expand the use of ECTs by enhancing the resolution and sensitivity of the visual record.

9.2 Saxophone Reed Inspection

Planar mesh-meander induction sensor was employed for non-destructive evaluation (NDE) of saxophone reeds. Reeds were rated on the following parameters: ease of attack, ease of sustenance, and tone quality in the low, middle, and high ranges of the instrument, as well as a score for volume. Figure 14 shows the types of saxophone reeds evaluated for the said parameters using planar mesh-meander planar electromagnetic system. Figure 15 displays the FR4 substrate based fabricated sensors for the mentioned application.

The frequency response obtained as a test of 8 different reeds show that the reeds with better tone quality behaved as resonant circuits with a peak obtained at 579 MHz as shown in the phase-shift vs frequency plot in Fig. 16.

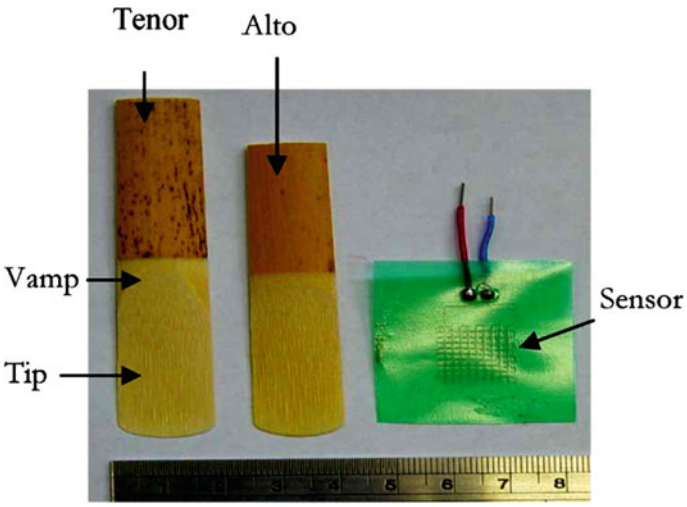

Fig. 14 A tenor and an alto saxophone reeds [29]

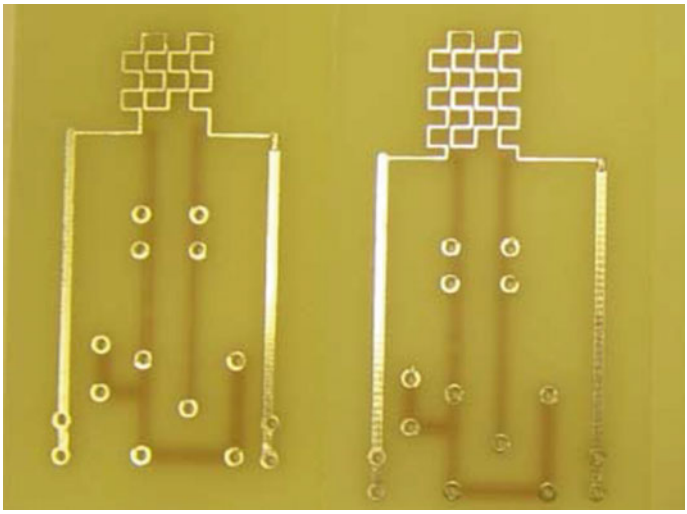

Fig. 15 FR4 substrate mesh sensor [29]

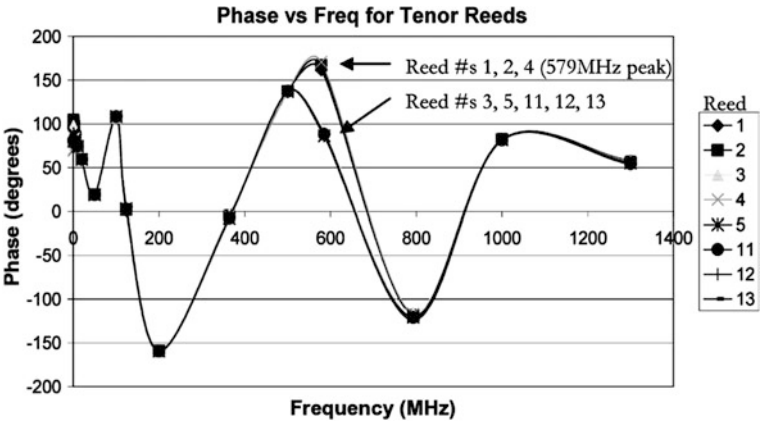

Fig. 16 Frequency response of tested reeds [29]

9.3 Planar Meander Sensors in Robotics

Pairs of meander coils were tested against angular displacements in a robotic foot, and results showed that the sensor gives correct information about displacement regardless how the foot touches the ground with its whole area. A planar meander-type sensor, where variation of input inductance serves as a measure of displacement, could be used as a ground reaction force (GRF) sensor to provide dynamic balance for legged locomotion. This inductive displacement sensor is constructed to detect normal, as well as tangential component of the force [33]. Figure 17 shows schematics of single-link actuated robotic foot and Fig. 18 shows the position of planar meander coil induction sensors in the robotic foot.

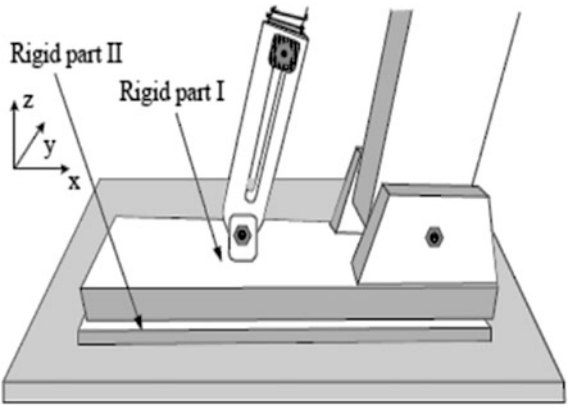

Fig. 17 Single-link robotic foot [33]

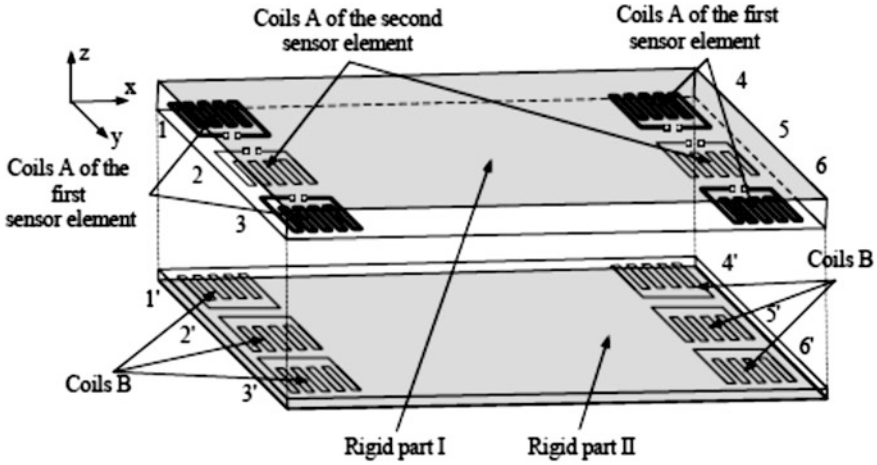

Fig. 18 Meander coil positioning in the foot [33]

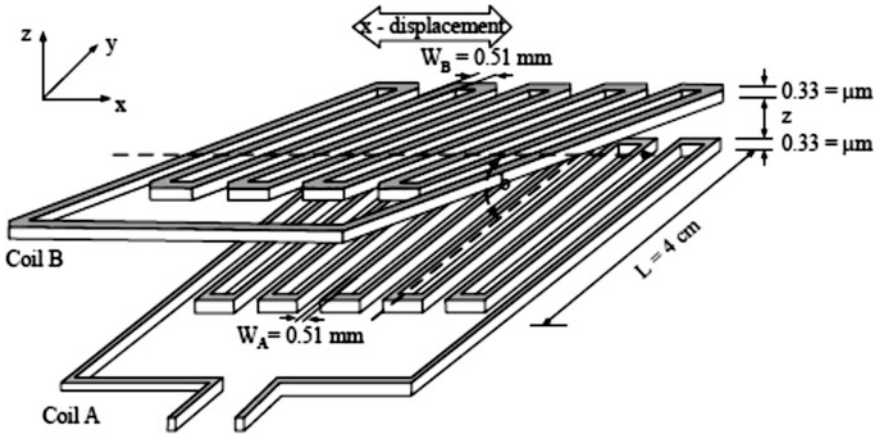

Fig. 19 Rotation of meander coil B about x-axis

Two most common cases were analyzed: when coil B rotates around x-axis for angle b (shown in Fig. 19) and around y-axis.

Impedance Analyzer HP4194A was used in the research to measure the inductive outcome from the meander sensing elements for different angles and distances between coils at the frequency of 1 MHz. The case results for x-axis rotations (i.e. for maximal angle β_{max} at particular distance), as shown in Fig. 20, for normal and tangential displacement. Calculated deviation between characteristics for maximal angle ($\beta = \beta_{max}$) and for the case when coils are parallel ($\beta = 0$) is

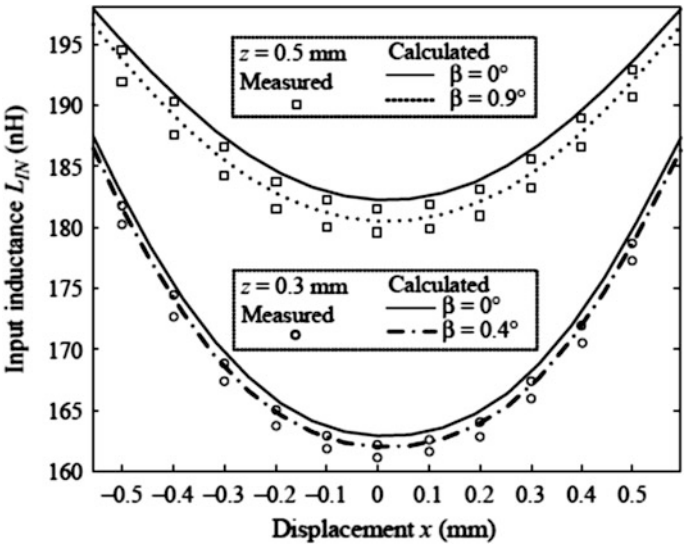

Fig. 20 Measured and calculated values of input inductance LIN when coil B rotates around x-axis [33]

shown in Fig. 20. Results reveal that these deviations are negligible concluding that the planar meander induction sensors provide the dependable information about the foot displacement, regardless how it touches the ground exposing the complete foot area to ground [33].

10 Conclusions

We have tried to showcase the recent advances in magnetic field planar sensors that could be used to measure magnetic field enjoying the privilege of non-destructive measurements and single side access to the sample. A trade-off between the sensor's size and its parameters measurement capability has always been accepted so far. With the increasing demand of miniaturization, low power consumption, compactness and portability of magnetometers, sensor size is often the only selection criterion. Applications, such as magnetic micro-beads, micro-magnetic scanning, non-destructive testing and medical applications like magnetic drug delivery urge the need of magnetic sensors that are smaller in size and own single side measurement capability. To cater those needs, it is utmost important to explore and apply new principles governing nano-scale science and technology.

References

1. A. Mahdi, L. Panina, D. Mapps, Some new horizons in magnetic sensing: high-T c SQUIDs, GMR and GMI materials. Sens. Actuators, A **105**, 271–285 (2003)
2. S.M. Sze, *Semiconductor Sensors* (Wiley, New York, 1994)
3. P. Ripka, Sensors based on bulk soft magnetic materials: advances and challenges. J. Magn. Magn. Mater. **320**, 2466–2473 (2008)
4. A. Ozbay, E. Nowak, A. Edelstein, G. Fischer, C. Nordman, S.F. Cheng, Magnetic-field dependence of the noise in a magnetoresistive sensor having MEMS flux concentrators. Trans. Magn. IEEE **42**, 3306–3308 (2006)
5. W. Lee, M. Toney, D. Mauri, High magnetoresistance in sputtered permalloy thin films through growth on seed layers of (Ni 0.81 Fe 0.19) 1-x Cr x. Trans. Magn. IEEE **36**, 381–385 (2000)
6. P. Ciureanu, S. Middelhoek, *Thin film resistive sensors* (CRC Press, Boca Raton, 1992)
7. R.S. Popovic, *Hall effect devices* (CRC Press, Boca Raton, 2003)
8. P. Ripka, M. Janošek, *Advances in magnetic field sensors* (2010)
9. C. Lei, R. Wang, Y. Zhou, Z. Zhou, MEMS micro fluxgate sensors with mutual vertical excitation coils and detection coils. Microsyst. Technol. **15**, 969–972 (2009)
10. Y. Haddab, V. Mosser, M. Lysowec, J. Suski, L. Demeus, C. Renaux, D. Flandre, in *Low-noise SOI Hall devices*, *SPIE's First International Symposium on Fluctuations and Noise* (2003), pp. 196–203
11. A. Kerlain, V. Mosser, Low frequency noise suppression in III-V Hall magnetic microsystems with integrated switches. Sens. Lett. **5**, 192–195 (2007)
12. P. Kejik, G. Boero, M. Demierre, R. Popovic, An integrated micro-hall probe for scanning magnetic microscopy. Sens. Actuators, A **129**, 212–215 (2006)
13. J. Lenz, A.S. Edelstein, Magnetic sensors and their applications. Sens. J. IEEE **6**, 631–649 (2006)
14. A. Bertoldi, D. Bassi, L. Ricci, D. Covi, S. Varas, Magnetoresistive magnetometer with improved bandwidth and response characteristics. Rev. Sci. Instrum. **76**, 065106-065106-6 (2005)
15. C.-C. Lu, J. Huang, P.-K. Chiu, S.-L. Chiu, J.-T. Jeng, High-sensitivity low-noise miniature fluxgate magnetometers using a flip chip conceptual design. Sensors **14**, 13815–13829 (2014)
16. Y. Cai, J. Qiu, L. Jiang, Planar three-axis magnetometer (2013)
17. S. Mukhopadhyay, Development of a novel planar mesh type micro-magnetic sensor for the quality inspection of electroplated materials. Sens. 2002 Proc. IEEE **2002**, 741–746 (2002)
18. S. Vernon, The universal impedance diagram of the ferrite pot core eddy current transducer. Trans. Magn. IEEE **25**, 2639–2645 (1989)
19. J. Bowler, H. Sabbagh, L. Sabbagh, The reduced impedance function for cup-core eddy-current probes. Trans. Magn. IEEE **25**, 2646–2649 (1989)
20. J.C. Moulder, E. Uzal, J.H. Rose, Thickness and conductivity of metallic layers from eddy current measurements. Rev. Sci. Instrum. **63**, 3455–3465 (1992)
21. S.C. Mukhopadhyay, S. Yamada, M. Iwahara, Investigation of near-surface material properties using planar type meander coil. JSAEM Stud. Appl. Electromagnet. Mech. **11**, 61–69 (2001)
22. S.C. Mukhopadhyay, Planar electromagnetic sensors: characterization, applications and experimental results (Planare elektromagnetische Sensoren: Charakterisierung, Anwendungen und experimentelle Ergebnisse). Tm-Technisches Messen **74**, 290–297 (2007)
23. S. Mukhopadhyay, C. Gooneratne, G.S. Gupta, S. Yamada, Characterization and comparative evaluation of novel planar electromagnetic sensors. Trans. Magn. IEEE **41**, 3658–3660 (2005)
24. N.J. Goldfine, K.G. Rhoads, K.E. Walrath, D.C. Clark, *Method for characterizing coating and substrates*. Google Patents, (2002)
25. N.J. Goldfine, Conformable, meandering winding magnetometer (MWM) for flaw and materials characterization in ferrous and nonferrous metals. Am. Soc. Mech. Eng. Press. Vessels Pip. Div. (Publication) PVP **352**, 39–43 (1997)

26. N.J. Goldfine, Magnetometers for improved materials characterization in aerospace applications. Mater. Eval. **51**, 396–405 (1993)
27. S. Yamada, M. Katou, M. Iwahara, F.P. Dawson, Defect images by planar ECT probe of Meander-Mesh coils. Trans. Magn. IEEE **32**, 4956–4958 (1996)
28. S.C. Mukhopadhyay, C.P. Gooneratne, G.S. Gupta, S.N. Demidenko, A low-cost sensing system for quality monitoring of dairy products. IEEE Trans. Instrum. Meas. **55**, 1331–1338 (2006)
29. S.C. Mukhopadhyay, G.S. Gupta, J.D. Woolley, S.N. Demidenko, Saxophone reed inspection employing planar electromagnetic sensors. IEEE Trans. Instrum. Meas. **56**, 2492–2503 (2007)
30. M.A.M. Yunus, S.C. Mukhopadhyay, Novel planar electromagnetic sensors for detection of nitrates and contamination in natural water sources. IEEE Sens. J **11**, 1440–1447 (2011)
31. A.R.M. Syaifudin, P. Yu, S. Mukhopadhyay, M.J. Haji-Sheikh, J. Vanderford, *Performance evaluation of a new novel planar interdigital sensors* (2010), pp. 731–736
32. M.A.M. Yunus, G.R. Mendez, S.C. Mukhopadhyay, Development of a low cost system for nitrate and contamination detections in natural water supply based on a planar electromagnetic sensor. Instrum. Measur. Technol. Conf. (I2MTC), 2011 IEEE **2011**, 1–6 (2011)
33. S.M. Djuric, L.F. Nagy, M.S. Damnjanovic, N.M. Djuric, L.D. Zivanov, A novel application of planar-type meander sensors. Microelectron. Int. **28**, 41–49 (2011)